

# Modified xonotlite-type calcium silicate hydrate slabs for fire doors

Journal of Fire Sciences

2018, Vol. 36(2) 83–96

© The Author(s) 2018

Reprints and permissions:

[sagepub.co.uk/journalsPermissions.nav](http://sagepub.co.uk/journalsPermissions.nav)

DOI: 10.1177/0734904118754381

[journals.sagepub.com/home/jfs](http://journals.sagepub.com/home/jfs)

Rimantas Levinskas<sup>1</sup>, Irena Lukošūtė<sup>1</sup>, Arūnas Baltušnikas<sup>1</sup>, Algirdas Kuoga<sup>2</sup>, Aldona Luobikienė<sup>3</sup>, José Rodríguez<sup>4</sup>, Inmaculada Cañadas<sup>4</sup> and Witold Brostow<sup>5</sup>

Date received: 23 October 2017; accepted: 29 December 2017

## Abstract

Xonotlite-type calcium silicate hydrate slabs were examined under the thermal shock conditions in a solar furnace at the Plataforma Solar de Almeria which can reach a peak of 300 W/cm<sup>2</sup>. We have studied the original slabs as well as those modified with a mixture of liquid sodium silicate including montmorillonite as thermal insulation materials for fire doors applications. The slabs were kept at 950°C for 1 h. We performed X-ray diffraction, thermogravimetry and differential scanning calorimetry analysis, scanning electron microscopy, Fourier transform infrared spectroscopy, and thermal conductivity measurements and determined N<sub>2</sub> adsorption/desorption isotherms. X-ray diffraction shows that during the thermal shock at 950°C xonotlite is converted to wollastonite. Specific surface areas of xonotlite slabs decrease due to release of crystalline water molecules. It is possible to maintain temperatures of the back door not exceeding 70°C while the front door is subjected to 950°C for 1-h time periods. The standard requires no more than 140°C at the back door.

## Keywords

Xonotlite slabs, solar energy, high temperature resistance, fire doors

<sup>1</sup>Laboratory of Material Research and Testing, Lithuanian Energy Institute, Kaunas, Lithuania

<sup>2</sup>Idomus Joint Stock Company, Kaunas, Lithuania

<sup>3</sup>Kaunas University of Technology, Kaunas, Lithuania

<sup>4</sup>Plataforma Solar de Almeria, Tabernas, Almeria, Spain

<sup>5</sup>LAPOM, Department of Materials Science & Engineering, University of North Texas, Denton, TX, USA

## Corresponding authors:

Witold Brostow, LAPOM, Department of Materials Science & Engineering, University of North Texas, 3940 North Elm Street, Denton, TX 76207, USA.

Email: [wkbrostow@gmail.com](mailto:wkbrostow@gmail.com)

## Introduction

Fighting fires is necessarily as old as humanity. As discussed by Eric Guillaume et al.,<sup>1</sup> understanding a fire involves "... the complex interactions between combustion chemistry, fluid dynamics and heat transfer." When, in 1824, Sadi Carnot<sup>2</sup> published his "Réflexions sur la puissance motrice du feu," his publication is believed to be the beginning of the science of thermodynamics.<sup>1,3</sup> Fire sciences consist of several areas, such as, for instance, estimation of species concentration during a fire studied by Julie Lassus et al.<sup>4</sup> In this work, we study the thermal insulation materials for fire doors under the conditions of a thermal shock. The thermal shock is provided by a solar furnace.

Calcium silicate hydrate phases such as tobermorite and xonotlite are important binding agents in building materials including concrete and lime-sand stone.<sup>5,6</sup> One can obtain calcium silicate hydrate at room temperature with the relative humidity of 60% in a reaction between the silicate phases of Portland cement and water, or else during the replacement of cement with a pozzolan, such as a fly ash from coal power plants and/or different types of aggregates.<sup>5,7,8</sup> Synthesis of pure tobermorite and xonotlite is possible in hyper-alkaline and hydrothermal conditions only.<sup>9,10</sup> Especially, xonotlite-based materials are suitable for many high-temperature applications due to their high thermal shock resistance and also chemical durability. Thus, examination of the light-weight xonotlite-tobermorite-based shells impregnated by epoxies composition has demonstrated good resistance to high-temperature gas flow initiated by a plasma jet.<sup>11</sup> We note that such new light and high-temperature resistant materials can be used in the aerospace industry as well as for construction purposes.<sup>3,12,13</sup>

Calcium sulfate dihydrate (gypsum) or calcium silicates are usually used in fire-protection constructions.<sup>14</sup> During exposure to high temperature, gypsum undergoes transformation into hemihydrate and anhydrite, a process accompanied by thermal shrinkage. Silica was used as a filler for the improvement of the thermal, physical, and mechanical properties of gypsum and also for reduction of the cracks formation.<sup>15</sup> The fire resistance of fire doors formed with gypsum plates and a stone wool layer was investigated.<sup>16</sup> It turns out that the long-term resistance of the doors is determined by the thickness of the rock wool, mass of gypsum, and the numbers of gypsum plates.<sup>16</sup>

Silica aerogel is a highly nano-porous material with low thermal conductivity; it has been widely used in heat storage and transport systems as well as for heat protection of space vehicles.<sup>17,18</sup> Heat protection can be also provided by porous polymers from high internal phase emulsions developed by Silverstein et al.<sup>19</sup>

Cement-based materials are widely used to protect concrete structures against fire. Portland cement-based mortars with 45% or 10% clinoptilolite substitution have compressive strength exceeding 42.5 MPa after being subjected to 400°C and 500°C.<sup>20</sup> One of the eco-friendly compositions prepared from a mixture of polypropylene fibers, porcelain, and blast furnace slag as a cement replacement displays excellent fire resistance.<sup>21</sup>

Passive fire-protection compositions have been developed to insulate the load-bearing substrates from fire. Such materials have low thermal conductivity related to nano-scale porosity; they generate their thermal resistance by immobilizing the gas molecules within their structures.<sup>22</sup>

The most widely used insulating material for fire-stop systems contains inorganic fibers such as stone wool. Fibrous materials have high fire resistance and can be used up to 1000°C in applications ranging from building constructions to ship building.<sup>23</sup> However, stone wool is not considered environmentally friendly. Xonotlite has a low thermal conductivity and

high strength in a wide temperature range.<sup>24–26</sup> Thus, xonotlite and related calcium silicate minerals added to plaster boards improve the fire resistance and raise the temperature at which the plaster boards ignite.<sup>27</sup>

The aim of this work was investigation of behavior and properties of modified calcium silicate hydrate (xonotlite) compositions at 950°C as thermal insulation materials suitable for the fire doors application. The pertinent European Standard is EN 13501.<sup>28</sup> As stated in the first section of the document,

The harmonized European Fire Standards are a set of test standards that have been accepted by all countries within the European Economic Community. This allows manufacturers to produce or import products that have been tested to a common standard without the need to test in each member state. Testing to these standards is now accepted in all ECC countries. Compliance with the European standards and regulations is mandatory.

ECC is the European Economic Community, with 28 countries as members. The key criteria defined by the EN 13501 Standard are the following ones:

- The structural element should not collapse or deflect beyond the permitted levels when subjected to the applied load.
- The integrity of the room must be maintained. No breakthrough of flames is permitted.
- The temperature on the non-exposed side of the structural element must not rise more than 140°C above ambient as an average measurement and no more than 180°C at any one location.

We have used concentrated solar energy to achieve and maintain the high temperatures needed.

## Experiment

As a mineral, xonotlite is monoclinic, with the chemical formula  $\text{Ca}_6\text{Si}_6\text{O}_{17}(\text{OH})_2$ . It was commercially available as xonotlite slabs with low density (250–300 kg/m<sup>3</sup>) and high strength (1.4 MPa) for construction of insulation layers for wood fires. Samples of xonotlite-type calcium silicate hydrate (50 mm × 50 mm × 50 mm) were modified with a mixture of sodium metasilicate, 5 wt% of montmorillonite (composition called XSM5M) or 5 wt% of organically modified montmorillonite (composition called XSM5MM).

We use montmorillonite  $(\text{Na}, \text{Ca})_{0.33}(\text{Al}, \text{Mg})_2(\text{Si}_4\text{O}_{10})(\text{OH})_2 \cdot n\text{H}_2\text{O}$  with the following properties: specific surface area (see below)  $S_{\text{BET}} = 89 \text{ m}^2/\text{g}$ , specific weight of 2.2 g/cm<sup>3</sup>, and bulk density of 0.65 g/cm<sup>3</sup>. Montmorillonite modified with a quaternary ammonium salt is characterized by  $S_{\text{BET}}$  of 5 m<sup>2</sup>/g, specific weight of 1.7 g/cm<sup>3</sup>, and bulk density of 0.45 g/cm<sup>3</sup>. Homogeneous dispersions for surface modification of samples were prepared by CAT X520 stirrer at  $1.1 \times 10^4$  r/min velocity during 120 s blending of montmorillonite or organically modified montmorillonite with sodium silicate solution (50%). Samples have been immersed into prepared dispersed material for 60 s to form a modified layer ≈2.5-mm thick. Previously, we have tried the immersion times of 30, 60, 90, and 120 s. After

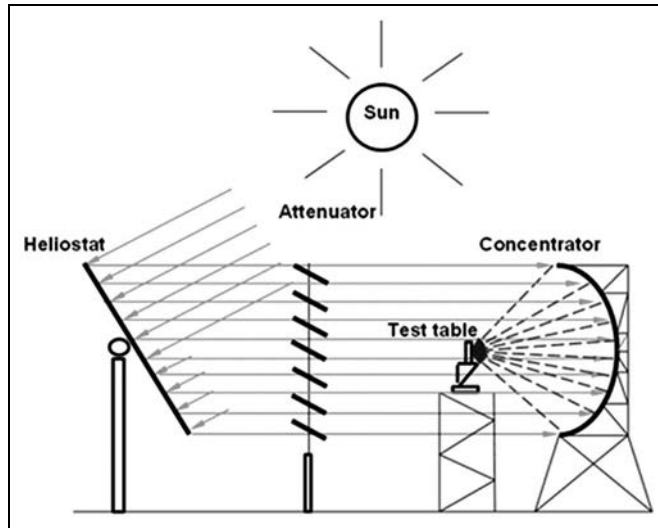


**Figure 1.** Functional sketch of the SF60 solar furnace at PSA.

desiccation, the samples immersed for 90 or 120 s had a negligible weight increase compared with the 60-s experiment, hence the decision of immersion time of 60 s.

Subsequently, the samples were dried at 30°C for 48 h so as to improve mechanical cohesion between slab particles on the sample surface. Lucas et al.<sup>29</sup> reported formation of adhesive bonds between silica and sodium silicate. We also recall that Roggendorf et al.<sup>30</sup> investigated pure liquid sodium silicate dried slowly and obtained amorphous materials with different contents of water. In our case, the liquid sodium silicate impregnated a  $\approx 5$ -mm deep layer of calcium silicate hydrate—filling pores between xonotlite crystals.

The samples cut away from xonotlite slab with the dimensions indicated and specially made fire-proof door elements (100 mm  $\times$  100 mm  $\times$  50 mm) were subjected to thermal shock in the SF60 Solar Furnace of the Plataforma Solar de Almeria (PSA) in Tabernas, province of Almeria, on the Mediterranean Sea in southern Spain. PSA is the largest research, development, and testing center in Europe dedicated to the concentration the solar energy. The SF60 solar furnace consists essentially of a flat 120-m<sup>2</sup> heliostat, a 100-m<sup>2</sup> parabolic concentrator, an attenuator (shutter), and a test table. The platform is able to intensify the natural solar beam of 25-cm diameter with the energy density over 300 W/cm<sup>2</sup> which can heat up the specimens above 2000°C.<sup>31,32</sup> This is due to geometrical properties of the parabola when the heliostat tracks the sun continuously and reflects its rays horizontally and parallel (without concentration) to the optical axis of the parabolic concentrator; the latter, in turn, concentrates the incoming rays onto the focus of the parabola. The amount of sunlight reflected toward the concentrator is regulated by the attenuator (shutter), located between the concentrator and the heliostat.<sup>33</sup> A functional sketch of the installation is shown in Figure 1.

The samples were placed on a metallic holder which was fixed to the test table. In this way, the samples were positioned at the focus by a three-axis displacement of the test table. Each sample was provided with two type K thermocouples, one in the front side (the exposed surface) and the other in the rear side. In order to expose just the front side of the specimen,

an alumina plaque with a square hole of the required size of the sample was placed in its front side. At least three tests were performed for each set of conditions.

X-ray diffraction (XRD) analysis of the samples was performed using a diffractometer equipped with a pyrolytic graphite monochromator for separation of  $\text{CuK}\alpha$  radiation. A goniometer was calibrated by corundum  $\alpha\text{-Al}_2\text{O}_3$  (99.9%) standard obtained from Alfa Aesar. Diffraction patterns were recorded using a Bragg-Brentano diffractometer at the voltage of 35 kV and emission current of 20 mA. X-ray scanning was carried out at a step size of  $0.01^\circ$  ( $2\theta$ ).

Simultaneous thermal analysis (thermogravimetry analysis and differential scanning calorimetry (TGA/DSC)) was performed on a Linseis STA PT1600 instrument. Finely ground samples of 15–17 mg were heated in a Pt-Rh crucible from  $25^\circ\text{C}$  to  $1000^\circ\text{C}$  at a heating rate of  $10^\circ\text{C}/\text{min}$  under air atmosphere. The differential thermogravimetric (DTG) curves were derived from thermogravimetric (TG) curves. Thermogravimetric analysis is explained for instance in Chapter 15 of Brostow and Hagg Lobland.<sup>3</sup>

Samples of xonotlite slabs were characterized by Fourier transform infrared spectroscopy (FTIR). FTIR spectra in the  $4000\text{--}550\text{ cm}^{-1}$  range were recorded by a Bruker Tensor 27 spectrophotometer with ATR-A537 (ZnSe) and TE-DLaTGS detector with a resolution of  $4\text{ cm}^{-1}$ .

The porosity characteristics and specific surface areas  $S_{\text{BET}}$  of our samples were measured by  $\text{N}_2$  adsorption/desorption using a Autosorb iQ Quantachrome volumetric sorption analyzer. All the samples were outgassed at  $95^\circ\text{C}$  for 12 h prior to measurements.  $S_{\text{BET}}$  was calculated by multi-point method using automatically selected points within the linear range of BET (Brunauer, Emmett, and Teller) equation. The total pore volume was determined at a relative pressure  $P/P_0 = 0.99$ , and pore size distribution was estimated by the density functional theory (DFT) method.

Microstructure analysis was carried out on a Zeiss EVO MA10 scanning electron microscope on the samples coated with gold in secondary electron mode and operated at 25 kV.

The thermal conductivities of xonotlite at different temperatures were measured by the hot wire method<sup>34</sup> that is especially appropriate for testing thermal insulation materials. Thermocouples are made from a chromel–alumel wire with 0.3-mm diameter. The hot wire and taps for voltage measurements are made of nichrome.

## Results and discussion

One option is the usage of stone wool as an insulation material for fire-proof doors with an optimal quantity of organic glue, usually a phenolic resin. Thus, experiments on elements of fire-stop systems created by the Idomus Company performed at the PSA demonstrate that the pyrolysis process does not pass through the entire thickness of samples during 1 h test at  $950^\circ\text{C}$ —as demonstrated in the following three figures.

We then moved on to xonotlite-containing slabs. An example of a sample kept at  $950^\circ\text{C}$  for 1 h is displayed in Figure 3.

We now compare results of using stone wool (Figure 2) and xonotlite-containing slabs (Figure 3). Looking along the middle axis of the specimen perpendicular to the length in Figure 2, we see that some 60% of material along that axis has suffered severe thermal degradation (gray color) what can be assigned to the phenolic resin pyrolysis. Some further (20%) suffered milder degradation (brownish color), apparently the organic resin not fully

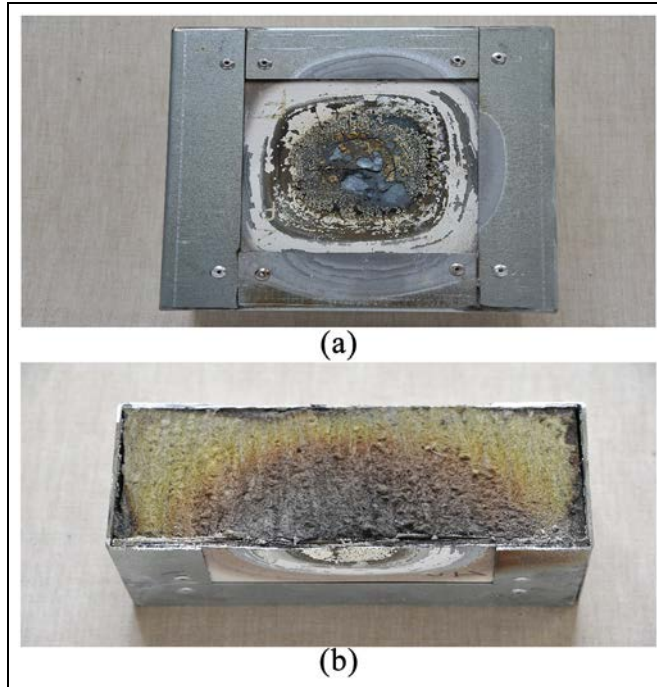


**Figure 2.** (a) A sample imitating a fire door element made of stone wool after solar irradiation and (b) a cross section of the tested sample (thickness of 100 mm) showing the depth influenced by the pyrolysis process in the sample at 950°C during 1 h.



**Figure 3.** A 50-mm-thick sample imitating a fire door element after solar irradiation maintaining 950°C for 1 h; a cross section (a side view similar to that in Figure 2).

degraded. Similar processes are noticed in thermal protection systems<sup>35,36</sup> such as those based on phenolic resin reinforced by graphite felt.<sup>35</sup> In other words, approximately 20% of

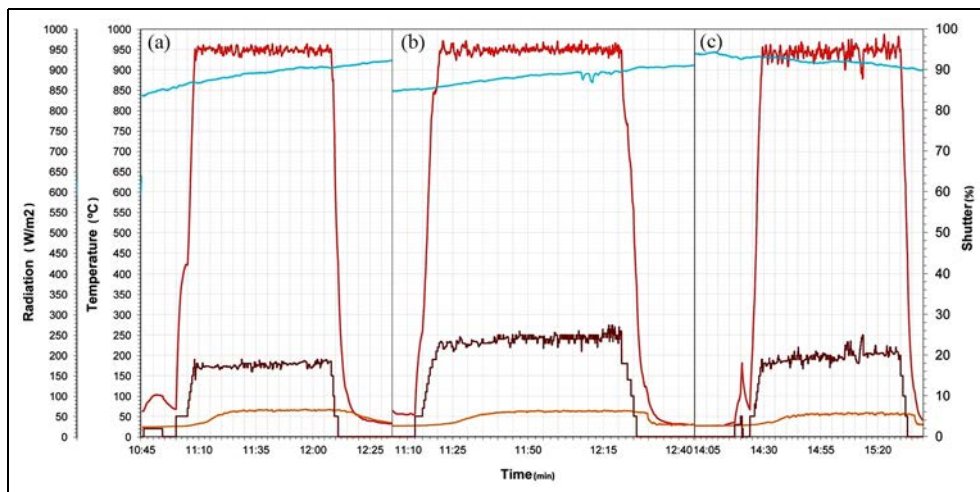


**Figure 4.** Temperature in °C of samples: front side (red line) and back side (orange line); and solar radiation in  $\text{W/m}^2$  (blue line) as functions of shutter opening in % (brown line) at real time of tests in min. Samples subjected to high-temperature treatments: 950°C applied as minimum for 1 h each time; (a) reference xonotlite slab without a modifying layer, (b) sodium silicate containing 5 wt% of montmorillonite (XSM5M), and (c) sodium silicate containing 5 wt% of organically modified montmorillonite (XSM5MM). Note the two vertical scales on the left.

the material along that axis appears unaffected. This is in sharp contrast to the xonotlite-containing slab in Figure 3; here, we see some 85% along that length axis unaffected by pyrolysis. Problems with thermal stability of stone wool fibers have been discussed by Yue et al.<sup>35</sup> along with some ways of stabilizing those fibers. The stone wool fibers do not necessarily retain their original geometric shapes at elevated temperatures. This while xonotlite represents a three-dimensional structure.

Results of three high-temperature treatment tests are shown in Figure 4. Figure 4(a) corresponds to a reference xonotlite slab without a modifying layer. The front walls of the samples were impregnated by liquid sodium silicate: Figure 4(b) shows sodium silicate contained 5 wt% of montmorillonite (XSM5M), and Figure 4(c) shows sodium silicate contained 5 wt% of organically modified montmorillonite (XSM5MM).

The results in Figure 4 in a way speak for themselves. The target of temperatures lower than 140°C at the back face has been exceeded. We are seeing temperatures not higher than 68°C in (a), not higher than 65°C in (b), and 55°C in (c). Incidentally, the use of the liquid sodium silicate mitigates dust formation in processing.

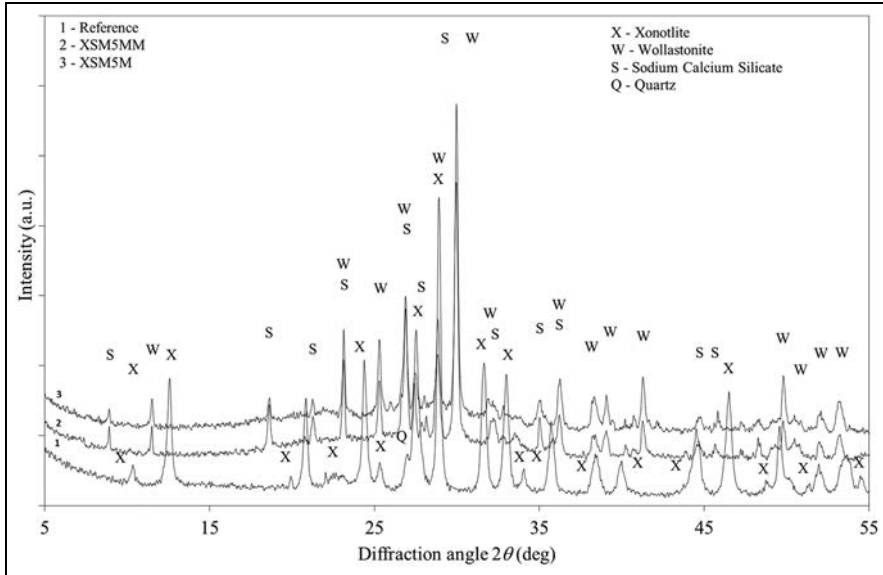
Since the success achieved is largely related to low thermal conductivity of xonotlite, in Table 1, we list the values of thermal conductivity  $\lambda$  at selected temperatures. These values were also obtained by averaging a minimum of three tests at each temperature.

We see in Table 1 an increase in thermal conductivity from the room temperature to 900°C by some 140%. This is a consequence of high-temperature dehydration of xonotlite resulting in formation of a denser phase of wollastonite.

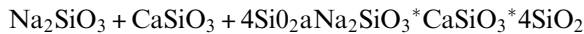
As noted in the Experiment section, we have also determined XRD patterns of our materials; see Figure 5.

**Table I.** Thermal conductivity of modified xonotlite (XSM5MM) at selected temperatures.

T (°C)	18	35	400	600	900
$\lambda$ (W/mK)	0.0791	0.0804	0.1079	0.1226	0.1910

**Figure 5.** XRD patterns: 1 for the reference material and after thermal shock, 2 for modified composition XSM5MM, and 3 for modified composition XSM5M.

In Figure 5 we see four species. In the reference (curve 1) of course, xonotlite dominates, but there are some traces of quartz. However, for modified compositions after thermal shock (curves 2 and 3), we see wollastonite created by conversion from xonotlite. We also see sodium calcium silicate as a product of a reaction between sodium silicate, wollastonite, and quartz. Namely



We now consider cumulative surface areas of pores of xonotlite and xonotlite after the thermal shock; see Figure 6.

We see in Figure 6 that the surface area of xonotlite = 20.6 m<sup>2</sup>/g, decreased to 5.3 m<sup>2</sup>/g as a consequence of the thermal shock and the resulting release of water molecules. Decrease in the number and cumulative surface area of the pores is also a consequence of that shock.

TGA (red) and DSC (black) results are jointly presented in Figure 7.

We see in Figure 7 that the relative mass change of xonotlite in the temperature range 30°C–930°C amounts to 16.5% (curve 1). This is another manifestation of the conversion of xonotlite to wollastonite. The endothermic effect at 30°C–330°C is related to adsorbed water



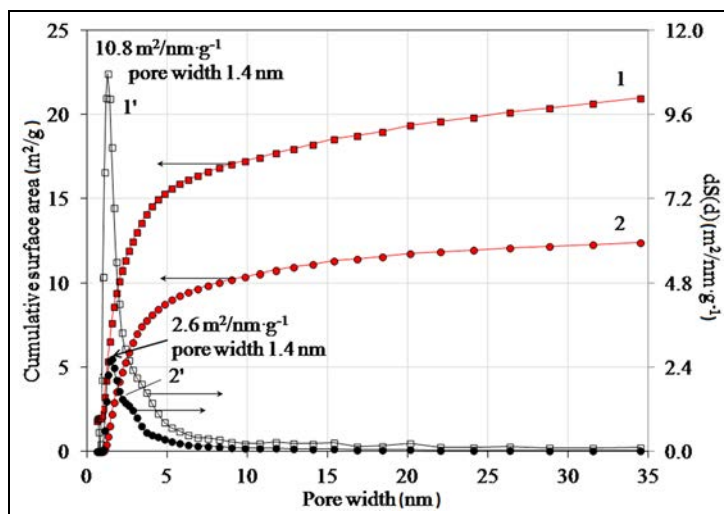


**Figure 6.** Cumulative surface area of pores (red) and surface area of prevalent pores with width of 1.4 nm (black) as a function of pore width. Curves 1 and 1' are for reference xonotlite; 2 and 2' for xonotlite after the thermal shock.

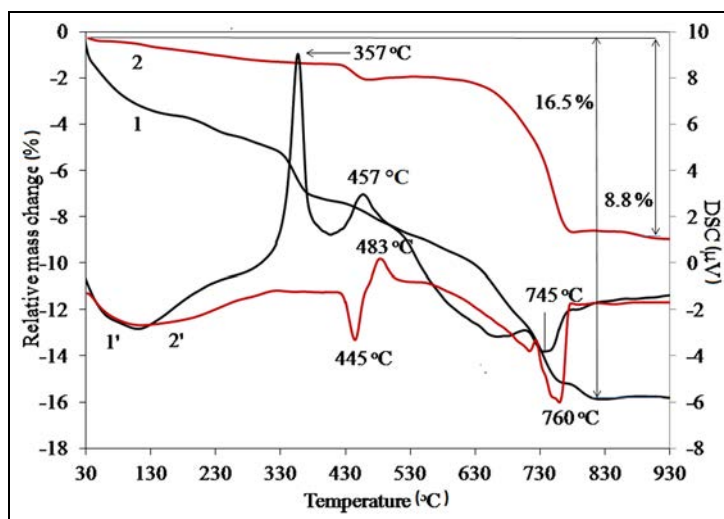


**Figure 7.** TGA and DSC results. Curves: 1 is TGA and 1' is DSC of the reference material, 2 is TGA and 2' is DSC after thermal shock; the latter sample was taken at the depth of 5–8 mm.

removal, while at 420°C–445°C we see the effect of endothermic initial water removal from large xonotlite crystals. We see the water removal effect with the highest speed of disintegration of xonotlite at 745°C–760°C. These effects and exothermal effect of crystallization of wollastonite at 810°C were reported by Spudulis et al.<sup>37</sup>. Šiaučiūnas et al.<sup>38</sup> reported

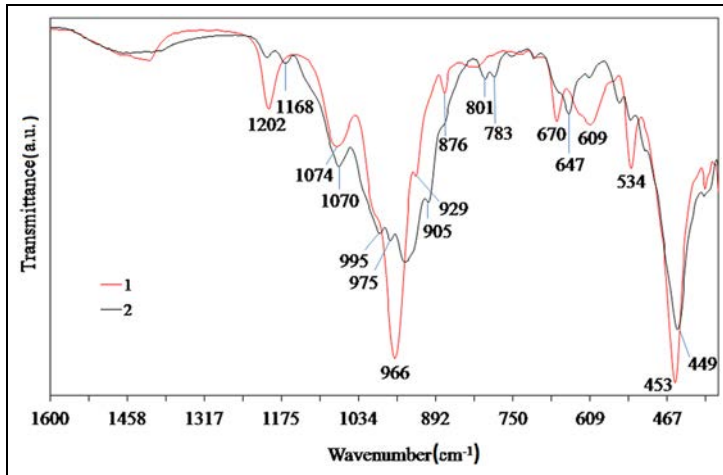


**Figure 8.** FTIR spectra of xonotlite before (curve 1) and after (curve 2) thermal shock.

formation of wollastonite starting around 775°C during the burning of a mixture of bedrock and marlstone.

Exothermal effects around 357°C and 457°C reflect two-step decomposition of organic substances (cellulose), which usually is seen during manufacturing xonotlite slabs. After the thermal shock, the relative mass change of xonotlite in the range 30°C–930°C amounts to 8.8% (curve 2). This is related to the removal of water from incomplete conversion of xonotlite to wollastonite. FTIR results are presented in Figure 8.

The strong absorption bands at 449–453 and 800–1200  $\text{cm}^{-1}$  mainly occur due to Si–O and O–Si–O vibrations, respectively. A sharp peak at 1202  $\text{cm}^{-1}$  is characteristic only for xonotlite before the thermal shock. After the shock, we see some new bands at 647, 783, 801, 975, 995, 1070, and 1168  $\text{cm}^{-1}$ . Their presence is assigned to wollastonite generated by high temperature.<sup>39</sup> The intensity of the absorption bands at 966 and 453  $\text{cm}^{-1}$  decreased due to de-hydroxylation of xonotlite at thermal shock conditions resulting in relative changes of the amounts of Si–O and O–Si–O groups. Selected scanning electron microscopy (SEM) results are presented in Figure 9.

Michler and Balta-Calleja<sup>40</sup> and Michler<sup>41</sup> explain in some detail how SEM observations can be understood. Our SEM data show crystals characteristic for the xonotlite needle structure (a). The particles of wollastonite formed after the thermal shock are highly heterogeneous and agglomerated (b). Furthermore, there is a small quantity of small particles adhering to the surfaces of the large grains. The conversion to wollastonite crystals is not complete. Somewhat further with formation of wollastonite after calcination went Yazdani and coworkers<sup>42</sup> who at 1000°C used nanosilica. Such silica enhances the formation of hydrate phases.

## Concluding remarks

We have noted above discussing Figure 4 how well our results comply also with the European standard EN 13501. The highest temperature at the back face was 68°C.

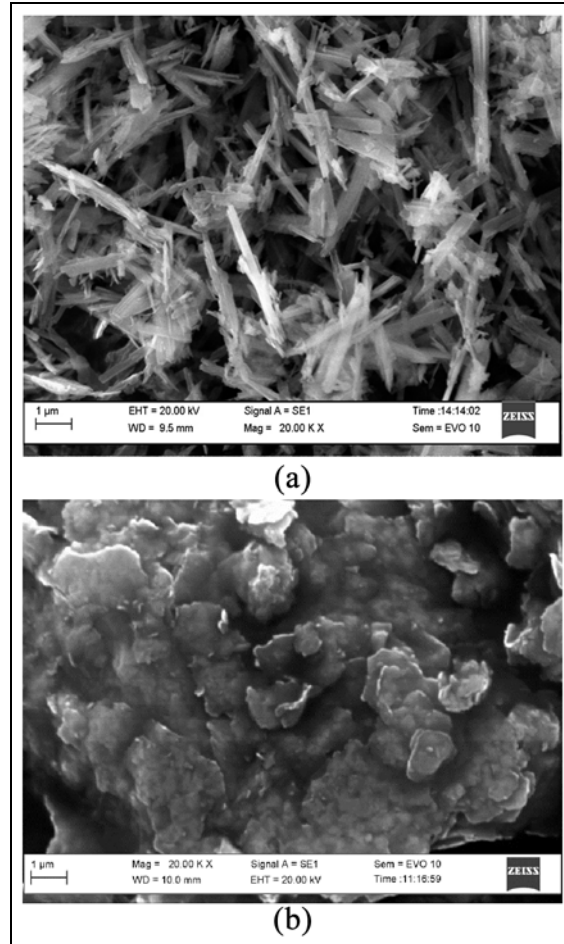


**Figure 9.** Scanning electron micrographs of xonotlite slabs: (a) before and (b) after the thermal shock.

As noted in the beginning of section “Experiment,” xonotlite-type calcium silicate hydrates exhibit low density, high strength and low thermal conductivity. As also already noted above, such materials are useful in aerospace systems.<sup>3,12,13</sup> We find that the same materials provide an attractive option for fire-stop systems. Slabs made from this material modified with sodium silicate including additives of montmorillonite and modified montmorillonite have demonstrated strong structural resistivity to the attack of high-energy sunlight. During the exposure for 1 h to 950°C temperature, the back face temperature was not higher than 70°C.

We further conclude that the use of the PSA facility with concentrated solar energy provided a highly useful and also a rapid method for finding suitable insulation materials for fire-proof doors. Because of its special working characteristics and the high sunlight concentration attained, this facility is suitable for tests in which the samples are heated up to a high temperature in a few seconds—as in our case where the fire-proof door slabs are submitted to a thermal shock.

## Acknowledgements

Service of the technical staff of Plataforma Solar de Almeria is gratefully acknowledged.

## Declaration of conflicting interests

The authors declared no potential conflicts of interest with respect to the research, authorship, and/or publication of this article.

## Funding

The authors disclosed receipt of the following financial support for the research, authorship, and/or publication of this article: This work was supported by the Access to Research Infrastructures activity of the European Union in the projects SFERA (grant no. 228296) and SFERA-II (grant no. 312643), Brussels.

## References

- Guillaume E, Marlair G, Delacroix A, Drysdale D. Considerations on combustion and fire behaviour of materials: a change of mind during the 18th century. *J Fire Sci* 2016; 34: 69–84.
- Carnot S. *Réflexions sur la puissance motrice du feu et sur les machines propres à développer cette puissance*. Paris: Chez Bachelier, 1824.
- Brostow W and Hagg Lobland HE. *Materials: Introduction and applications*. New York: John Wiley & Sons, 2017.
- Lassus J, Courty L, Garo J-P, Studer E, Jourda P, Aine Ph. Estimation of species concentrations during a fire in a reduced-scale room. *J Fire Sci* 2016; 34: 30–50.
- Tekin I, Durgun MY, Gencel O, Bilir T, Brostow W, Hagg Lobland HE. Concretes with synthetic aggregates for sustainability. *Constr Build Mater* 2017; 133: 425–432.
- Hartmann A, Schulenberg D and Buhl J-C. Synthesis and structural characterization of CSH-phases in the range of C/S = 0.41–1.66 at temperatures of the tobermorite xonotlite crossover. *J Mater Sci Chem Eng* 2015; 3: 39–55.
- Gencel O, Koksall F, Ozel C, Brostow W. Combined effects of fly ash and waste ferrochromium on properties of concrete. *Constr Build Mater* 2012; 29: 633–640.
- Uygunoglu T, Topcu IB, Gencel O, Brostow W. The effect of fly ash content and types of aggregates on the properties of pre-fabricated concrete interlocking blocks (PCIBs). *Constr Build Mater* 2012; 30: 180–187.
- Shaw S, Clark SM and Henderson CBM. Hydrothermal formation of calcium silicate hydrates, tobermorite ( $\text{Ca}_5\text{Si}_6\text{O}_{16}(\text{OH})_2 \cdot 4\text{H}_2\text{O}$ ) and xonotlite ( $\text{Ca}_6\text{Si}_6\text{O}_{17}(\text{OH})_2$ ): an in situ synchrotron study. *Chem Geol* 2000; 167: 129–140.
- Hartmann A, Schulenberg D and Buhl J-C. Investigation of the transition reaction of tobermorite to xonotlite under influence of additives. *Adv Chem Eng Sci* 2015; 5: 197–214.
- Levinskas R, Kėzelis R, Brinkienė K, et al. High temperature ablation of composite material under plasma jet impact. *Mater Sci Medžiagotyra* 2011; 17: 423–427.
- Venkatapathy E, Laub B, Hartman GJ, et al. Thermal protection system development, testing, and qualification for atmospheric probes and sample return missions: examples for Saturn, Titan and Stardust-type sample return. *Adv Space Res* 2009; 44: 138–150.
- Cao J, Zhang Y and Zeng L. Preparation of nonporous super thermal insulation material compounded with xonotlite-SiO<sub>2</sub>-aerogel and characterization of the pore structure. *Key Eng Mater* 2007; 336–338: 1505–1508.
- Baux C, Mélinge Y, Lanos C, Jaubertie R. Enhanced gypsum panels for fire protection. *J Mater Civil Eng* 2008; 20: 71–77.
- Féjean J, Lanos C, Meçlinge Y, Baux C. Behaviour of fire-proofing materials containing gypsum, modifications induced by incorporation of inert filler. *Chem Eng Res Des* 2003; 81: 1230–1236.
- Lausmaa T. Correlation of the fire resistance time of fire doors and the structure of fire doors. In: *Proceedings of 6th Baltic Heat Transfer Conference*, Tampere, August 24–26, 2011, pp. 1–8.
- Berthon-Fabry S, Hildenbrand C, Ilbizan P, Jones E, Tavera S. Evaluation of lightweight and flexible insulating aerogel blankets based on Resorcinol-Formaldehyde-Silica for space applications. *Eur Polym J* 2017; 93: 403–416.
- Rosa F, Valverde A, Aranda JM, Aranda J, Rodriguez J. CESA-1 project capabilities for high temperature material testing: application to the HERMES wing leading edge tests. *Sol Energy* 1991; 46: 175–182.
- Silverstein MS, Tai H, Sergienko A, Lumelsky Y, Pavlovsky S. PolyHIPE: IPNs, hybrids, nanoscale porosity, silica monoliths and ICP-based sensors. *Polymer* 2005; 46: 6682–6694.
- Beycioglu A, Aruntas HY, Gencel O, Hagg Lobland HE, Samandar A, Brostow W. Effect of elevated temperatures on properties of blended cements with clinoptilolite. *Mater Sci Medžiagotyra* 2016; 22: 548–552.
- Won J-P, Kang H-B, Lee S-J, Kang Y-W. Eco-friendly fire proof high-strength polymer cementitious composites. *Constr Build Mater* 2012; 30: 406–412.
- Christke S, Gibson AG, Grigoriou K, Mouritz AP. Multi-layer polymer metal laminates for the fire protection of lightweight structures. *Mater Design* 2016; 97: 349–356.
- Karamanos A, Papadopoulos A and Anastasellos D. Heat transfer phenomena in fibrous insulating materials, [http://aix.meng.auth.gr; http://www.geolan.gr/sappek/docs/publications/article\\_6.pdf](http://aix.meng.auth.gr; http://www.geolan.gr/sappek/docs/publications/article_6.pdf)
- Churakov SV and Mandaliev P. Structure of the hydrogen bonds and silica defects in the tetrahedral double chain of xonotlite. *Cement Concrete Res* 2008; 38: 300–311.

25. Wei G, Zhang X and Yu F. Thermal conductivity of xonotlite insulation material. *Int J Thermophys* 2007; 28: 1718–1729.
26. Milestone NB and Ahari GK. Hydrothermal processing of xonotlite based compositions. *Adv Appl Ceram* 2007; 106: 302–308.
27. Frost RL, Mahendran M, Poologanathan K, Xi Y. Raman spectroscopic study of the mineral xonotlite  $\text{Ca}_6\text{Si}_6\text{O}_{17}(\text{OH})_2$ —a component of plaster boards. *Mater Res Bull* 2012; 47: 3644–3649.
28. Fire: EN 13501—the European Standard, [http://www.owa.de/docs/pdf/DS\\_9500\\_eu\\_e\\_Fire\\_resistance\\_051400.pdf](http://www.owa.de/docs/pdf/DS_9500_eu_e_Fire_resistance_051400.pdf)
29. Lucas S, Tognonvi MT, Gelet J-L, Soro J, Rossignol S. Interaction between silica sand and sodium silicate solution during consolidation process. *J Non-Cryst Solids* 2011; 357: 1310–1318.
30. Roggendorf H, Boschel D and Rodicker B. Differential scanning calorimetry at hydrothermal conditions of amorphous materials prepared by drying sodium silicate solutions. *J Therm Anal Calorim* 2001; 63: 641–652.
31. Rodriguez J, Martinez D, Guerra Rosa L, Cruz Fernandes J, Amaral PM, Shohoji N. Photochemical effects in carbide synthesis of d-group transition metals (Ti, Zr; V, Nb, Ta; Cr, Mo, W) in a solar furnace at PSA (Plataforma Solar de Almeria). *J Sol Energ: T ASME* 2000; 123: 109–116.
32. Oliveira FAC, Shohoji N, Cruz Fernandes J, Guerra Rosa L. Solar sintering of cordierite-based ceramics at low temperatures. *Sol Energy* 2005; 78: 351–361.
33. Rodriguez J, Cañadas I and Zarza E. New PSA high concentration solar furnace SF40. *AIP Conf Proc* 2016; 1734: 070028.
34. ISO 8894-1:2010. Refractory materials—determination of thermal conductivity—part 1: hot-wire methods (cross-array and resistance thermometer).
35. Yue Y, Korsgaard M, Frank Kirkegaard L, Heide G. Formation of a nanocrystalline layer on the surface of stone wool fibers. *J Am Ceram Soc* 2008; 92: 62–67.
36. Pulci G, Tirillo J, Marra F, Fossati F, Bartuli C, Valente T. Carbon–phenolic ablative materials for re-entry space vehicles: manufacturing and properties. *Compos Part A: Appl S* 2010; 41: 1483–1490.
37. Spudulis E, Savareika V and Spokauskas A. Influence of hydrothermal synthesis condition on xonotlite crystal morphology. *Mater Sci Medžiagotyra* 2013; 19: 190–196.
38. Šiaučiusas R, Gendvilas R and Mikaliūnaitė J, Urbonas L. Application of isomorphous Ca-Si rocks for the synthesis of  $\alpha$ -C2S hydrate. *Mater Sci Medžiagotyra* 2014; 20: 321–326.
39. Zhao W, Zhang Q and Peng C. FTIR spectra for molecular structure of wollastonite. *J Chin Ceram Soc* 2006; 9: 1137–1139.
40. Michler GH and Balta-Calleja FJ. *Nano- and micromechanics of polymers: structure modification and improvement of properties*. Munich; Cincinnati, OH: Hanser, 2012.
41. Michler GH. *Atlas of polymer structures*. Munich; Cincinnati, OH: Hanser, 2016.
42. Yazdani A, Rezaie HR, Ghassai H, Mahmoudian M. The effect of processing parameters on the hydrothermal synthesis of wollastonite at low pressure. *J Ceram Process Res* 2013; 14: 12–16.

## Author biographies

**Rimantas Levinskas** is a Senior Researcher at the Laboratory of Materials Research and Testing of the Lithuanian Energy Institute. He is PhD of technological sciences-materials engineering. Research areas: high temperature resistant materials, composites, their properties and behavior in high temperatures gas and plasma flows.

**Irena Lukošiuūtė** is a Head of Laboratory of Material Research and Testing at the Lithuanian Energy Institute. She has a PhD in Technological Sciences-Materials Engineering. Research areas: polymer and composite science and engineering, nanofillers, development and research of multifunctional materials and composites, reliability of power plant facilities- research of materials aging processes and degradation of properties due to the impact of operational factors.

**Arūnas Baltušnikas** is a Senior Researcher at the Laboratory of Material Research and Testing of the Lithuanian Energy Institute. He has PhD in Technological Sciences-Materials Engineering. Research areas: X-ray powder diffraction analysis, nanocomposites, nanofillers, reliability of power plant facilities- research of metal aging processes and degradation of properties due to the impact of high temperatures.

**Algirdas Kuoga** is the General Manager and owner of Idomus Joint Stock Company. Areas of interests: fireproof doors and gates, new materials and technical solutions for preventing fire spread in industrial and civil buildings.

**Aldona Luobikienė** is a Lecturer in the Construction Technologies Department, College of Construction and Architecture, Kaunas University of Technology. Her main research interests:

conflict analysis between construction participants from the legal standpoint, basics of Construction Laws, property law and insurance, construction agreements.

**José Rodríguez García** is a Facility Manager of the PSA Solar Furnace -High flux Concentration Facility at the Plataforma Solar de Almería -PSA-CIEMAT. He graduated in Mechanical Technical Engineering from the Escuela Politécnica Superior in Córdoba, Spain, in 1982. After eight years of work in Plataforma Solar de Almería as Tests Supervisor in Central Towers and Parabolic Trough systems, he joined CIEMAT in 1991 and became a member of the Concentrated Solar System Unit in PSA-CIEMAT. He is currently involved in Solar Thermal Treatment of Materials and in the production of Solar Heat for Industrial Processes.

**Inmaculada Cañadas Martínez** has a degree in Chemical Engineering and a PhD in Engineering from the University of Seville, Spain. She is a researcher at Plataforma Solar de Almería-CIEMAT as member of the Concentrated Solar Systems Unit. She has 17 years of experience in materials treatment and high temperature solar heat generation for industrial processes in solar furnaces. She has participated in more than 11 research & development projects, 9 national and trans-national access projects, and 3 collaboration agreements. She is co-author of more than 25 papers in SCI journals and more than 60 communications to national and international conferences.

**Witold Brostow** is Regents Professor of Materials Science and Engineering at the University of North Texas; Doctor of Science honoris causa, University of Lucknow; Member of the European Academy of Sciences, Brussels; Fellow of the Royal Society of Chemistry, London. He is President of Scientific Committee of the POLYCHAR World Forum on Advanced Materials (43 countries represented) and President of the International Council on Materials Education (16 countries represented). His research includes sustainable materials & their processing; tribology including friction and wear; fire resistance of materials and structures; drag reduction and flocculation; new approaches to instruction in Materials Science & Engineering.